The effect of Pb^{2+} substitution on the quantum paraelectric behaviour of $CaTiO_3$

2006 J. Phys.: Condens. Matter 18 2977

(http://iopscience.iop.org/0953-8984/18/11/005)

INSTITUTE OF PHYSICS PUBLISHING JOURNAL OF PHYSICS: CONDENSED MATTER

J. Phys.: Condens. Matter **18** (2006) 2977–2994 doi:10.1088/0953-8984/18/11/005

The effect of Pb^{2+} substitution on the quantum paraelectric behaviour of $CaTiO_3$

Amreesh Chandra[1], Rajeev Ranjan[1], D P Singh[2], Neeraj Khare[2] and Dhananjai Pandey[1]

[1] School of Materials Science and Technology, Institute of Technology, Banaras Hindu University, Varanasi-221005, India
[2] National Physical Laboratory, New Delhi, India

E-mail: dpandey@bhu.ac.in

Received 7 January 2006
Published 27 February 2006
Online at stacks.iop.org/JPhysCM/18/2977

Abstract

Temperature dependent dielectric, x-ray diffraction and '$1/f$' conductance noise studies on $(Ca_{1-x}Pb_x)TiO_3$ ceramics provide evidence for a new phase transition in this mixed system for the composition range $0.10 \leqslant x \leqslant 0.40$. The dielectric anomaly corresponding to this transition is superposed on the quantum paraelectric background of the host $CaTiO_3$ matrix. This anomaly is not associated with a ferroelectric or relaxor ferroelectric transition, as confirmed by the absence of a polarization hysteresis loop. The Curie–Weiss temperature for this transition is found to be negative which, using Kittel's model, is proposed to be due to an antiferroelectric transition. These results are discussed in the light of recently reported soft modes in $CaTiO_3$. It is also shown that the nature of phase transition changes abruptly from antiferroelectric to relaxor ferroelectric type at $0.40 < x < 0.45$ and finally to a normal ferroelectric type for $0.60 < x \leqslant 1.0$. The relaxor behaviour in the intermediate composition range is attributed to frustration caused by competing ferroelectric and antiferroelectric instabilities.

1. Introduction

Several materials like $KTaO_3$ [1, 2], $SrTiO_3$ [3], $CaTiO_3$ [4], TiO_2 [5], $X_{1/2}Na_{1/2}TiO_3$ (X = Dy, Ho, Er, Tm, Yb, Lu) [6] are known to exhibit quantum paraelectric behaviour. Amongst these, $SrTiO_3$, $CaTiO_3$ and TiO_2 are common ingredients of various ceramic capacitors [7]. In all these quantum paraelectrics, the dielectric ($\varepsilon'(T)$) initially increases with decreasing temperature in a Curie–Weiss manner but shows a departure from this behaviour at intermediate temperatures followed by saturation of the dielectric permittivity at very low temperatures. This low temperature saturation of the dielectric permittivity in quantum paraelectrics like $SrTiO_3$ and $KTaO_3$ has been attributed to the zero-point fluctuations of the lattice which precludes

condensation of the soft TO mode at $q = 0$ [3]. The possibility of a sharp transition around 40 K due to a coherent quantum state has also been proposed for $SrTiO_3$ [8–11]. There have been several theoretical efforts to understand these quantum effects in $SrTiO_3$ [3, 12–14]. Using path integral Monte Carlo simulations and an *ab initio* effective Hamiltonian, Zhong and Vanderbilt [14] have recently shown that the quantum fluctuations can indeed suppress the ferroelectric transition of $SrTiO_3$ completely.

The temperature variation of the dielectric permittivity in quantum paraelectrics has been fitted with the following quantum mechanical mean-field formula, originally due to Barrett [15]:

$$\varepsilon' \approx C/(T_1/2)\coth(T_1/2T) - T_c]. \tag{1}$$

This expression has been derived within the self-consistent single-mode theory for quantum crystals [3] as well as a limiting case of a renormalized harmonic approximation involving nonlinear polarizability of the oxygen shell [16]. The characteristic temperature T_1 in equation (1) signifies the onset of a low temperature regime in which the quantum effects are important and in which the dielectric permittivity shows deviation from the classical Curie–Weiss law. For temperatures $T > T_1$, where the quantum effects can be ignored, equation (1) reduces to the classical Curie–Weiss law with the T_c of equation (1) becoming the Curie–Weiss temperature. The values of T_c for $SrTiO_3$ and $KTaO_3$ are positive (38 and 13.1 K, respectively) [3, 16] whereas for materials like $CaTiO_3$ and TiO_2, T_c is found to be negative ($T_c = -159$ and -166 K, respectively) [4, 5]. At present, there is no satisfactory explanation as to why some quantum paraelectrics exhibit positive T_c values while others show negative ones.

The role of chemical substitutions in suppressing the quantum fluctuations has been extensively investigated for quantum paraelectrics with positive Curie–Weiss temperature. For example, chemical substitutions like A ($=Ca^{2+}$, Ba^{2+} or Pb^{2+}) in place of Sr^{2+} in the mixed system $(Sr_{1-x}A_x)TiO_3$ have been shown to suppress quantum fluctuations and stabilize a quantum ferroelectric phase with T_c varying as $(x - x_c)^{1/2}$, where $x_c \approx 0.002$ [17, 18]. In the $Sr_{1-x}Ca_xTiO_3$ system, the dielectric response gets smeared out for $0.016 \leqslant x \leqslant 0.12$ which has recently been attributed to competing ferroelectric and antiferroelectric instabilities [19, 20]. Further, for $0.12 \leqslant x \leqslant 0.40$, this system exhibits an antiferroelectric phase transition (AFE) [19, 21, 22]. Substitutions in place of K^+ in the mixed system $(K_{1-x}A_x)TaO_3$ (where A $= Li^{1+}$ or Na^{1+}) are also known to suppress the quantum fluctuations but, unlike for $(Sr_{1-x}Ca_x)TiO_3$, here a glassy polar phase is stabilized for $x_c \geqslant 0.01$ and 0.12 for Li^{1+} and Na^{1+}, respectively [1, 2]. On increasing their concentration beyond $x = 0.022$ and 0.20 for Li^{1+} and Na^{1+} substitutions, normal ferroelectric behaviour has been reported [1, 2]. Since the suppression of the quantum fluctuations eventually stabilizes a ferroelectric phase in both $SrTiO_3$ and $KTaO_3$, both of these have also been termed incipient ferroelectrics [1–3] which is consistent with the fact that the soft TO phonons with $q = 0$ have been observed in both the materials but this mode does not freeze out even at temperatures very close to $T = 0$ K [23, 24].

While the role of chemical substitutions in suppressing the quantum fluctuations has been investigated in some detail for $SrTiO_3$ and $KTaO_3$ with positive Curie–Weiss temperature, there are only two reports [25, 26] on the role of chemical substitutions in $CaTiO_3$ which, as said earlier, has a negative T_c. Lemanov *et al* [25] studied the effect of Pb^{2+} and Ba^{2+} substitutions in place of Ca^{2+} in the mixed system $(Ca_{1-x}A_x)TiO_3$ (A $= Pb^{2+}, Ba^{2+}$) for $x = 0.05$ and found that the quantum paraelectric behaviour still persists. In a more recent work on the $(Ca_{1-x}Pb_x)TiO_3$ system, Lemanov *et al* [26] have shown that the quantum paraelectric behaviour of $CaTiO_3$ persists for $x < 0.35$ while a relaxor ferroelectric phase,

similar to that reported earlier by Ranjan *et al* [27] for $x = 0.50$, appears for $x = 0.35$. We present here evidence for a new phase transition, not observed by earlier workers [26], in the mixed $(Ca_{1-x}Pb_x)TiO_3$ system for $x = 0.10, 0.20, 0.30$ and 0.40 (henceforth abbreviated as CPT10, CPT20, CPT30 and CPT40, respectively) using temperature dependent dielectric, x-ray diffraction and '$1/f$' conductance noise measurements. This new phase transition is shown to be of non-ferroelectric type. Results of dielectric and polarization measurements are also presented to show that this non-ferroelectric-type transition gives way to a relaxor-type transition for $x > 0.40$ and finally to the normal ferroelectric type for $x > 0.65$.

2. Experiment

It is quite important to prepare stoichiometric samples in order to understand the intrinsic behaviour of the CPT system. Lemanov *et al* [26] prepared the CPT powders by calcination at 1150 °C for 20 h in air. These powders will invariably be non-stoichiometric, as PbO vapour pressure is very high above 850 °C thereby causing large Pb^{2+} losses at the calcination stage itself, which cannot be recovered during sintering even if the sintering is done in a closed PbO atmosphere. In the present work, ceramic CPT samples were prepared by the solid state reaction route. Stoichiometric amounts of $PbCO_3$, $CaCO_3$ and TiO_2 powders were taken and mixed in a ball mill using zirconia jars and balls for 6 h. Acetone was used as a mixing medium. Calcination of mixed powders was carried out in two stages. The mixed powder was first calcined at 750 °C in air for 6 h to remove the volatile component (CO_2) of the mixture. This powder was again ball milled for 3 h and then recalcined at 900 °C for 6 h to ensure complete thermochemical reaction amongst the constituents to get single-phase material. To prevent the PbO loss, a second calcination was carried out in a sealed alumina crucible containing PbO atmosphere. The double-calcined powders were again ball milled for 2 h to break the agglomerates. The CPT powder so obtained was used for the preparation of disc shaped pellets, nearly 13 mm in diameter and 1.5 mm in thickness, at an optimized load of 70 kN using a few drops of 2% PVA solution as a binder. After the PVA burn-off at 500 °C, sintering was carried out at 1200 °C for 6 h in a sealed alumina crucible with PbO atmosphere to obtain ceramic samples with a percentage theoretical density of nearly 92% for pure CT and about 95% for CPT samples with $0 < x \leqslant 0.70$. For $x > 0.70$, the cubic to tetragonal transformation strain is so high that it leads to cracking of the ceramic pellets, as is well known for pure $PbTiO_3$ [28].

For dielectric and polarization measurements, both the faces of sintered pellets were gently polished with 0.25 μm diamond paste and then washed with acetone to clean the surface. Isopropyl alcohol was then applied to remove the moisture, if any, left on the pellet surface. Fired-on silver paste was subsequently applied on both the faces of the pellet. It was first dried at 100 °C in an oven and then cured by firing at 500 °C for 10 min. Dielectric measurements were carried out in the frequency range 10 kHz to 1 MHz using a Solartron 1290 Impedance Analyzer at an ac field of 1 V in the temperature range 300–4.2 K.

The polarization hysteresis loop measurements were carried out using a locally fabricated hysteresis loop tracer based on a modified Sawyer–Tower circuit in conjunction with a Agilent 54624A storage oscilloscope.

For collecting x-ray diffraction (XRD) data, sintered pellets were first crushed into fine powders. These crushed powders were then annealed at 500 °C for 10 h to remove strains which may develop during the process of crushing. These annealed powders were used for collecting the x-ray diffraction (XRD) data. Powder x-ray diffraction data were collected using a 18 kW Rigaku copper rotating anode based powder diffractometer (operating in the Bragg–Brentano geometry) fitted with a low temperature He closed cycle refrigerator (CCR) based attachment supplied by Rigaku capable of going down to 12 K and having a curved crystal

graphite monochromator in the diffracted beam. The data collection was done at 8 kW at a scan rate of 1° min^{-1} and step width of 0.01° in the 2θ range 20°–120°.

For conductance noise measurements, the voltage developed across the sample was amplified by a low noise amplifier (SRS, SR 560) and supplied to a dynamic signal analyser (HP3561A) for the analysis of the signal in the frequency domain mode. The sample temperature for the dielectric and conductance noise measurements was varied gradually by dipping the samples in liquid He and liquid N_2 cryocans, respectively.

3. Results and discussion

3.1. Dielectric studies

3.1.1. The composition range $0.0 \leqslant x \leqslant 0.40$. Figures 1(a)–(f) depict the variation of the real ($\varepsilon'(T)$) and imaginary ($\varepsilon''(T)$) parts of the dielectric permittivity of $CaTiO_3$ (CT), $Ca_{0.95}Pb_{0.05}TiO_3$ (CPT05), $Ca_{0.90}Pb_{0.10}TiO_3$ (CPT10) and $Ca_{0.80}Pb_{0.20}TiO_3$ (CPT20), $Ca_{0.70}Pb_{0.30}TiO_3$ (CPT30) and $Ca_{0.60}Pb_{0.40}TiO_3$ (CPT40), respectively, with temperature at a measuring frequency of 100 kHz. It is evident from figure 1(a) that for pure $CaTiO_3$, ε' increases with decreasing temperature as per Barrett's law [15] and shows quantum saturation below ∼50 K as expected for a quantum paraelectric and as observed by earlier workers also [4]. The Barrett fit is shown by solid line in figure 1. The nature of the $\varepsilon'(T)$ plot remains similar for $x = 0.05$ (figure 1(b)). For other CPT compositions with $0.10 \leqslant x \leqslant 0.40$, a small peak, superposed on the quantum paraelectric background, appears around 145, 175, 215 and 275 K for CPT10, CPT20, CPT30 and CPT40, respectively (figures 1(c)–(f)). The dielectric anomaly temperature increases with increasing Pb^{2+} content as shown in figure 2. It may be mentioned that the value of the dielectric permittivity at any temperature increases with increasing Pb^{2+} content. For example, the saturation dielectric permittivity increases from about 230 for pure CT to about 815 for CPT40 at 30 K whereas the room temperature value increases from 140 to 290. This may be attributed in part to the larger polarizability of Pb^{2+} as compared to Ca^{2+} as well as to the local strains produced as a result of difference in the ionic radii of Pb^{2+} (1.32 Å) and Ca^{2+} (0.99 Å).

The dielectric peak temperatures in figure 1 are found to be independent of the measuring frequency, and the temperatures T'_m and T''_m corresponding to the peaks in the real and the imaginary parts of the dielectric permittivity are coincident. This rules out the possibility of a dipole glass or relaxor transition, since for such transitions one expects $T''_m < T'_m$ for a given measuring frequency and also shifting of T'_m and T''_m to higher temperatures with increasing measuring frequency [29, 30].

It is interesting to note that if the small peaks in figure 1 are ignored, the entire $\varepsilon'(T)$ data set can still be fitted with Barret's formula, like for pure $CaTiO_3$. While fitting Barret's formula, it is important to remember that the values of the various constants of equation (1) must approximately satisfy the following constraints:

$$T_{sat} = T_1/2\sqrt{2} \tag{2}$$

$$\varepsilon(0) \approx C/[(T_1/2) - T_c] \approx C/[\sqrt{2}T_{sat} - T_c] \tag{3}$$

where T_{sat} is the temperature below which the dielectric permittivity becomes nearly temperature independent. In view of equations (2) and (3), the constants C, T_1 and T_c cannot be varied independently. This fact was kept in mind while fitting equation (1) to the observed experimental data shown in figure 1. Various parameters of Barrett's law so obtained are listed in table 1 for CT, CPT10, CPT20, CPT30 and CPT40 while their variation with x is shown in figure 3. It is worth mentioning that the values of the constants T_1 and T_c in equation (1) obtained by different workers for pure $CaTiO_3$ do not agree. Kim *et al* [4] have reported

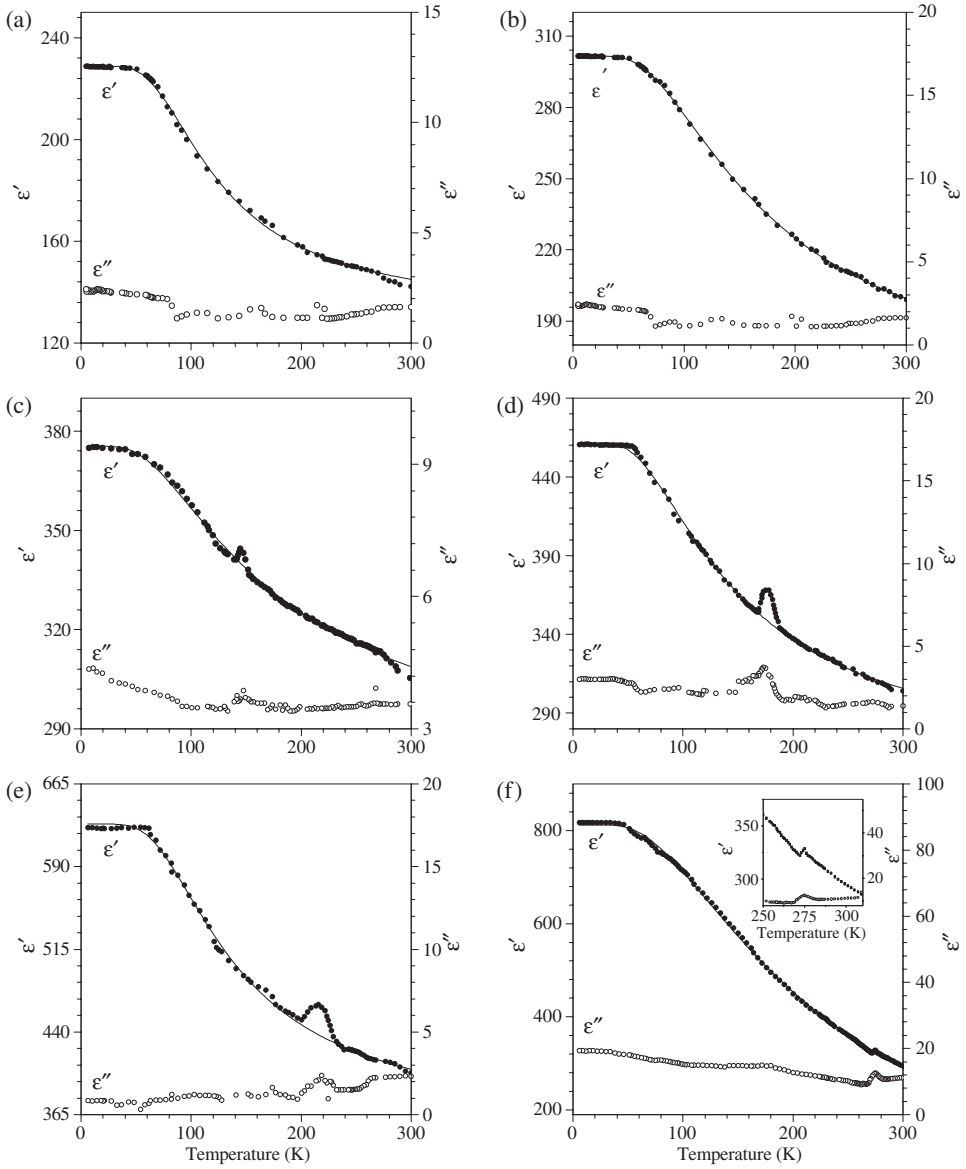

Figure 1. Variation of real (ε') and imaginary (ε'') parts of the dielectric permittivity at 100 kHz with temperature in $(Ca_{1-x}Pb_x)TiO_3$ with x equal to (a) 0.00, (b) 0.05 (c) 0.10 (d) 0.20 (e) 0.30 and (f) 0.40. The solid lines are the Barrett fits.

$T_1 = 104$ K and $T_c = -159$ K while Lemanov *et al* [25] have given $T_1 = 110$ K and $T_c = -111$ K. Our values of T_1 and T_c are 167 and -161, respectively, and satisfy the constraints given by equations (2) and (3).

It is evident from table 1 that unlike that of the characteristic temperature T_1, which changes only marginally with increasing Pb^{2+} content (about 21 K for $\Delta x = 0.40$), the value of the equivalent Curie–Weiss temperature (T_c) increases considerably and changes sign from negative to positive for $x > 0.40$, the significance of which will be discussed in later sections.

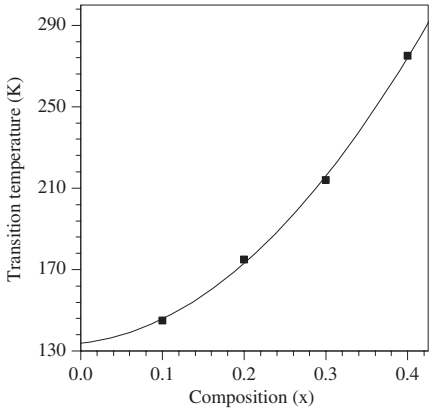

Figure 2. Variation of the transition temperature in the compositional range $0 < x < 0.45$.

Table 1. Variation of Barrett constants with composition (x).

Composition	C	T_1	T_c
CT	54 962	167.54	−161.45
CPT5	71 100	164.11	−155.22
CPT10	71 429	163.1	−110.29
CPT20	78 430	159.99	−91.54
CPT30	90 383	155.69	−67.89
CPT40	100 450	147.58	−31.32

3.1.2. The composition range $0.40 < x < 0.60$. On increasing the Pb^{2+} content further (i.e., for $0.40 < x < 0.60$), the temperature dependence of the dielectric permittivity ($\varepsilon'(T)$) changes dramatically. The variation of the real and imaginary parts of the dielectric permittivity for a representative composition $Ca_{0.55}Pb_{0.45}TiO_3$ (CPT45) is shown in figure 4 at six different frequencies (1 kHz, 10 kHz, 46 kHz, 100 kHz, 464 kHz and 1 MHz). A comparison of figure 4 with figure 1(f) shows that the quantum saturation of $\varepsilon'(T)$ for $x \leqslant 0.40$ has abruptly disappeared for $x > 0.40$. Instead, a very broad peak in the $\varepsilon'(T)$ plot is observed. Further, the peak temperatures T'_m and T''_m of the real and the imaginary parts of the dielectric permittivity are no longer coincident; instead $T''_m < T'_m$, a behaviour well known for relaxor ferroelectrics [29, 30]. However, in archetypal relaxors like $Pb(Mg_{1/3}Nb_{1/3})O_3$, T''_m is not only less than T'_m but both the characteristic temperatures show strong frequency dispersion at radio frequencies with T'_m and T''_m both shifting to higher temperatures on increasing the measuring frequency, which has usually been explained in terms of relaxational freezing of polar clusters as per the Vogel–Fulcher law [31]. For CPT45, these frequency dependent shifts are, however, rather small.

3.1.3. The composition range $0.60 < x \leqslant 1.0$. The dielectric measurements on CPT samples in the composition range $0.60 \leqslant x < 1.0$ show sharp peaks near the phase transition temperature as shown in figure 5 for one representative composition, $x = 0.65$. The peak value of $\varepsilon'(T)$ at T'_m is very much larger than that for CPT45. Further, both the characteristic temperatures, T'_m and T''_m, are not only coincident but are also frequency independent, as expected for a normal ferroelectric phase transition.

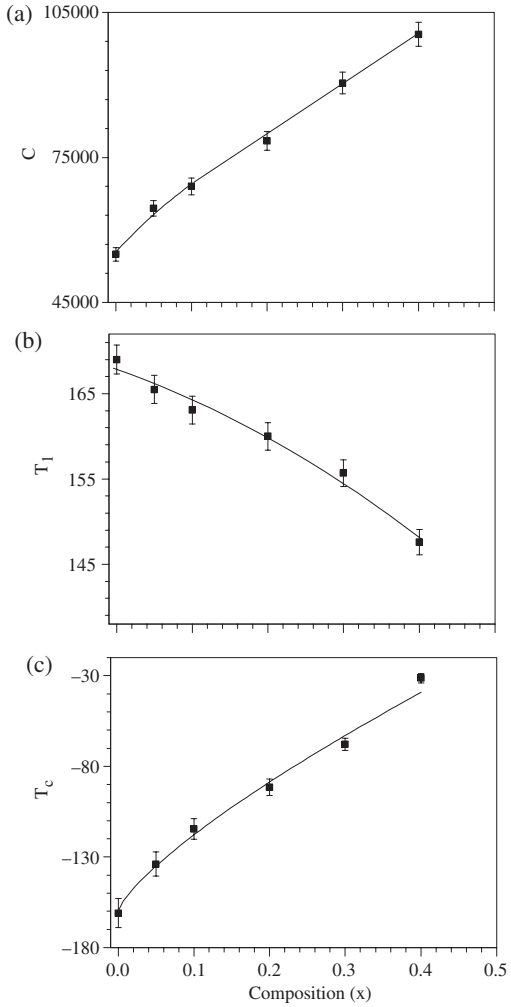

Figure 3. Variation of Barrett's constants in the composition range $0.00 \leqslant x \leqslant 0.40$.

3.2. Polarization studies

We have carried out temperature dependent polarization–electric field (P–E) hysteresis loop measurements in the three composition ranges discussed above in an effort to understand the origin of the dielectric anomalies in the three ranges. No hysteresis loop was observed below the transition temperature for fields up to 60 kV cm^{-1} for CPT10, CPT20, CPT30 and CPT40. This is illustrated in figure 6(a) which depicts a linear dependence of the polarization on the electric field for CPT20 at 150 K which is below the corresponding transition temperature T'_m (175 K). Dielectric breakdown of the samples occurred on application of fields greater than 60 kV cm^{-1}. It is worth mentioning that for both conventional ferroelectrics and dipolar glass/relaxor ferroelectric materials, an external field of 60 kV cm^{-1} is large enough to open up the hysteresis loop [2, 29, 30]. The absence of a hysteresis loop in the composition range $0.10 \leqslant x \leqslant 0.40$ rules out any ferroelectric or relaxor ferroelectric transition being responsible for the dielectric anomaly shown in figure 1.

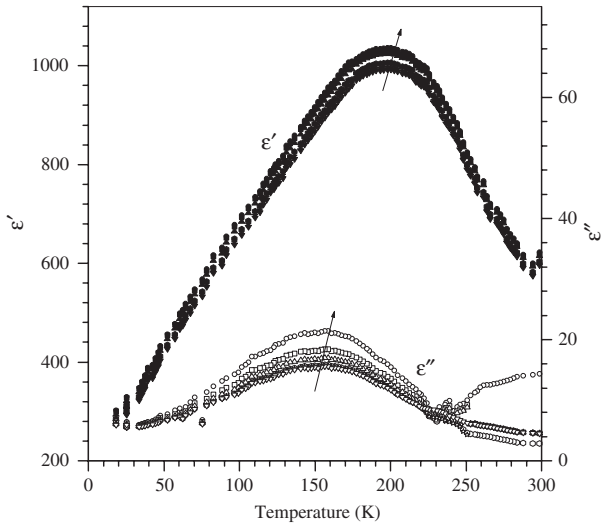

Figure 4. Variation of real (ε') and imaginary (ε'') parts of the dielectric permittivity at 1 kHz, 10 kHz, 46 kHz, 100 kHz, 464 kHz and 1 MHz with temperature for $(Ca_{1-x}Pb_x)TiO_3$ with $x = 0.45$.

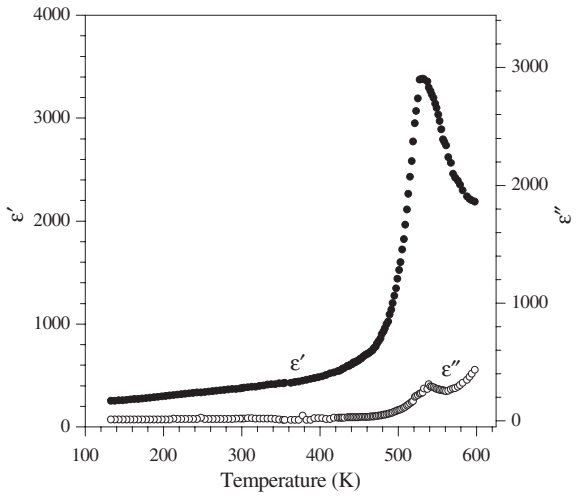

Figure 5. Variation of real (ε') and imaginary (ε'') parts of the dielectric permittivity at 100 kHz, with temperature for $(Ca_{1-x}Pb_x)TiO_3$ with $x = 0.65$.

For CPT45, we observe a slim hysteresis loop as shown in figure 6(b) at 150 K which is below the dielectric peak temperature T'_m (196 K). This slim loop for CPT45 persists even above T'_m, as expected for relaxor ferroelectrics [29, 30] and gradually opens up on lowering the temperature. This is illustrated in figure 7 which depicts the temperature evolution of the hysteresis loop for CPT45. The observation of a slim hysteresis loop above T'_m indicates the presence of field alignable clusters of dipoles even above T'_m. As is well known, for normal ferroelectrics, unlike relaxor ferroelectrics, the hysteresis loop disappears at the ferroelectric transition temperature (T'_m).

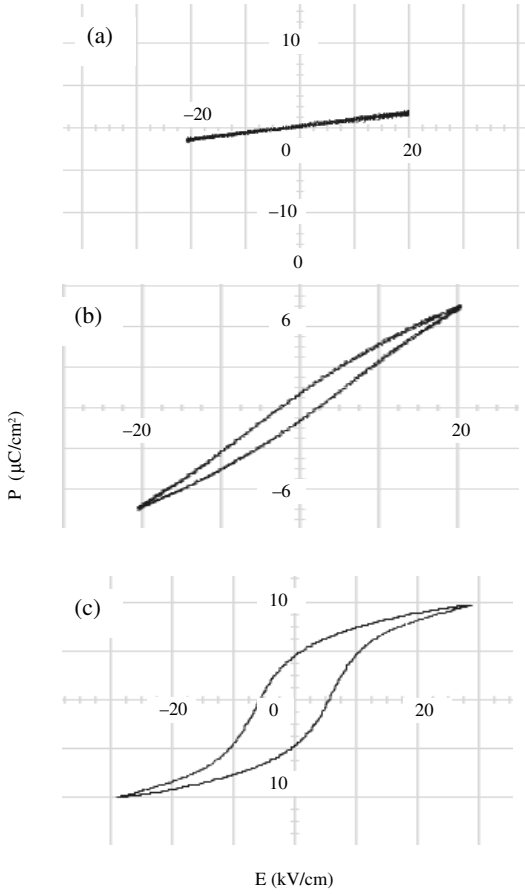

Figure 6. P–E hysteresis loop for ceramic samples of $(Ca_{1-x}Pb_x)TiO_3$ with x equal to (a) 0.20, (b) 0.45 and (c) 0.65 at 150 K.

In the composition range $0.65 \leqslant x \leqslant 1$, one observes a saturated hysteresis loop, as expected for a normal ferroelectric. This is illustrated in figure 6(c) for CPT65 at 150 K which is well below the transition temperature $T'_m = 532$ K. This observation confirms that the sharp dielectric anomaly shown in figure 5 is due to a normal ferroelectric transition.

3.3. Additional evidence for a phase transition in the composition range $0.0 \leqslant x \leqslant 0.40$

3.3.1. '1/f' Conductance noise studies. Further confirmation about the occurrence of a phase transition in CPT samples with $0.10 \leqslant x \leqslant 0.40$ was obtained by measuring the '$1/f$' conductance noise of the lattice across the phase transition temperature. Figure 8 shows the temperature dependence of the normalized conductance noise (S_v/V^2), where S_v is the voltage noise density and V is the voltage, in CPT20. From this figure, it is clearly seen that near the phase transition temperature, the level of noise increases and attains the peak value around the same temperature at which the anomalies in the dielectric permittivity occur. This increase in noise near the phase transition temperature can be attributed to the rearrangement of atomic positions taking place around the transition temperature. The conductance noise measurements thus provide additional confirmation for the occurrence of a phase transition in CPT with $0.10 \leqslant x \leqslant 0.40$.

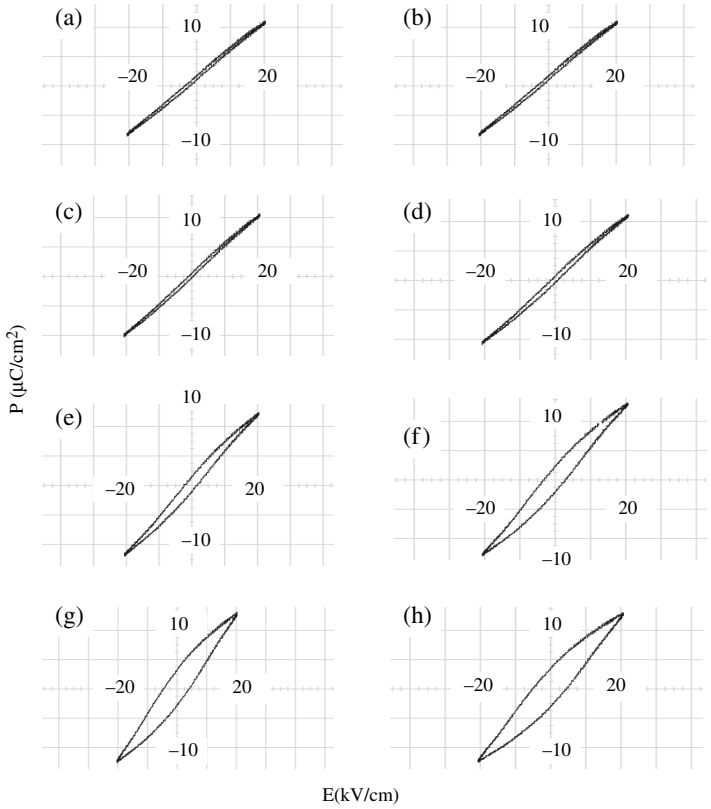

Figure 7. Temperature evolution of the P–E hysteresis loop for ceramic samples of $(Ca_{1-x}Pb_x)TiO_3$ with $x = 0.45$; (a) 243 K, (b) 223 K, (c) 213 K, (d) 200 K, (e) 183 K, (f) 163 K, (g) 143 K and (h) 133 K. Note that the loop increasingly opens up as the temperature in lowered.

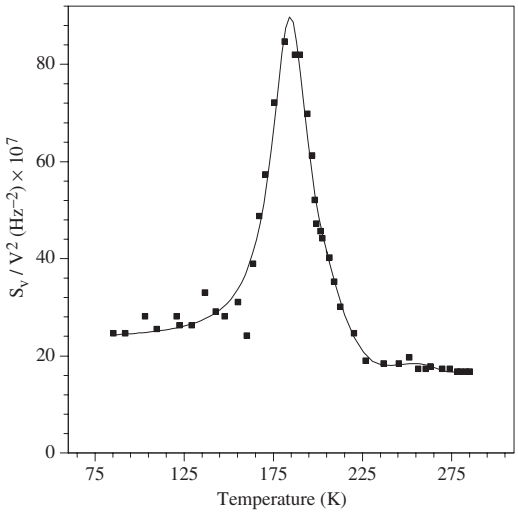

Figure 8. Variation of '$1/f$' conductance noise with temperature for $(Ca_{0.80}Pb_{0.20})TiO_3$.

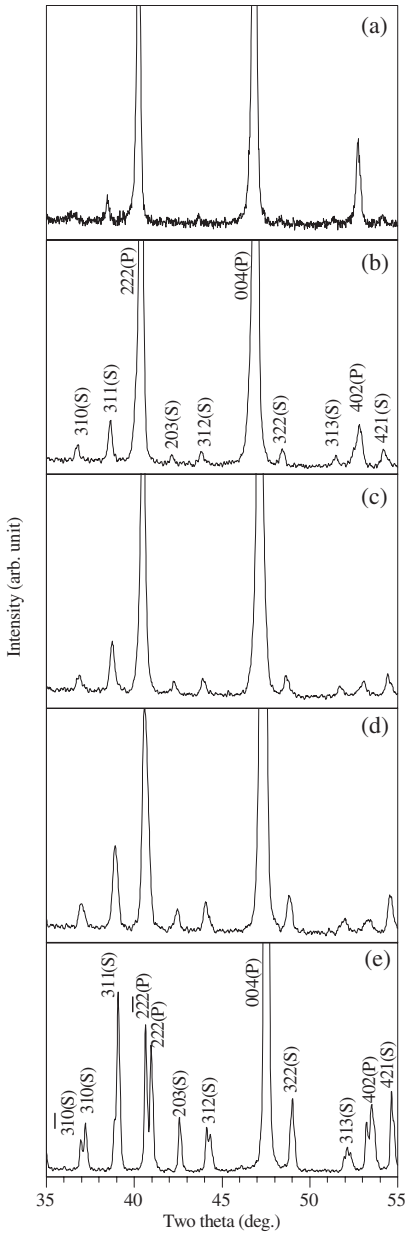

Figure 9. Evolution of the room temperature XRD pattern of $(Ca_{1-x}Pb_x)TiO_3$ with x equal to (a) 0.40, (b) 0.30, (c) 0.20, (d) 0.10 and (e) 0.00.

3.3.2. X-ray diffraction studies. Figure 9 depicts the room temperature powder XRD patterns of $(Ca_{1-x}Pb_x)TiO_3$ for $x = 0.40, 0.30, 0.20, 0.10$ and 0.00. The XRD patterns in figure 9 contain main perovskite as well as superlattice reflections marked as P and S, respectively. Both types of reflections can be indexed with respect to a doubled pseudocubic cell. With respect to such a cell, the elementary perovskite peaks assume *hkl* indices which are represented by all even (e) integers. The superlattice reflections, on the other hand, have one or more odd (o)

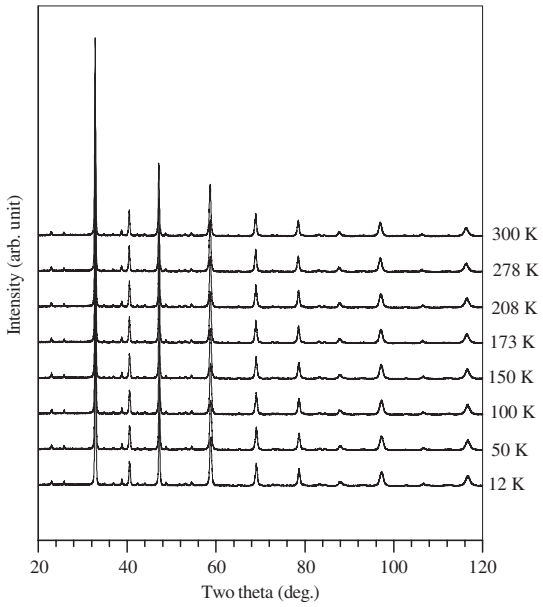

Figure 10. Temperature evolution of the powder XRD pattern of $Ca_{0.80}Pb_{0.20}TiO_3$.

numbered indices. The patterns shown in figure 9 contain superlattice reflections of the types ooo, ooe and oee (e.g. 311, 312, 322 in the figure) which are known to arise due to antiphase octahedral tilts, in-phase octahedral tilts and antiparallel cationic (Ca^{2+}/Pb^{2+}) displacements, respectively, as explained by Glazer [32]. Since all the perovskite (P) and superlattice (S) peaks are common for $0 \leqslant x \leqslant 0.40$, we conclude that in this composition range there is no change in the room temperature structure of $CaTiO_3$ as a result of Pb^{2+} substitution, i.e., the crystal structure of the paraelectric phase of CPT remains orthorhombic with the *Pbnm* space group and $a^-a^-c^+$ tilt system [33] over the entire composition range $0.0 \leqslant x \leqslant 0.40$. The structure becomes tetragonal (i.e., $PbTiO_3$ like) for $x \geqslant 0.58$ whereas for $0.40 < x < 0.58$, the orthorhombic and tetragonal phases are found to coexist [33].

In the low temperature XRD studies on CPT with $0.10 \leqslant x \leqslant 0.40$, we did not observe any new superlattice peaks below the dielectric anomaly temperature other than those already present above T'_m due to the octahedral tilts and antiparallel cationic shifts, discussed in the previous paragraph. This is illustrated in figure 10, which depicts the temperature evolution of the XRD pattern for CPT20. In fact, Rietveld analysis of the powder XRD data in the 2θ range 20°–120° using the *Pbnm* space group give satisfactory fits at all the temperatures. However, the orthorhombic cell parameters obtained by Rietveld refinement at various temperatures using the room temperature *Pbnm* space group reveal a small but distinct discontinuous change in the '*a*' and '*b*' unit cell parameters as well as the unit cell volume as shown in figure 11. This discontinuous change in the *a* and *b* parameters and the cell volume suggests a weakly first-order transition. Further, this discontinuous change occurs at the same temperature at which the dielectric anomaly is seen in figure 1(d). Thus the XRD studies provide one more piece of evidence for the occurrence of a phase transition.

3.4. Discussion

3.4.1. Curie–Weiss dependence of the dielectric permittivity in the composition range $0.10 \leqslant x \leqslant 0.40$. The absence of the P–E hysteresis loop below the transition temperature for

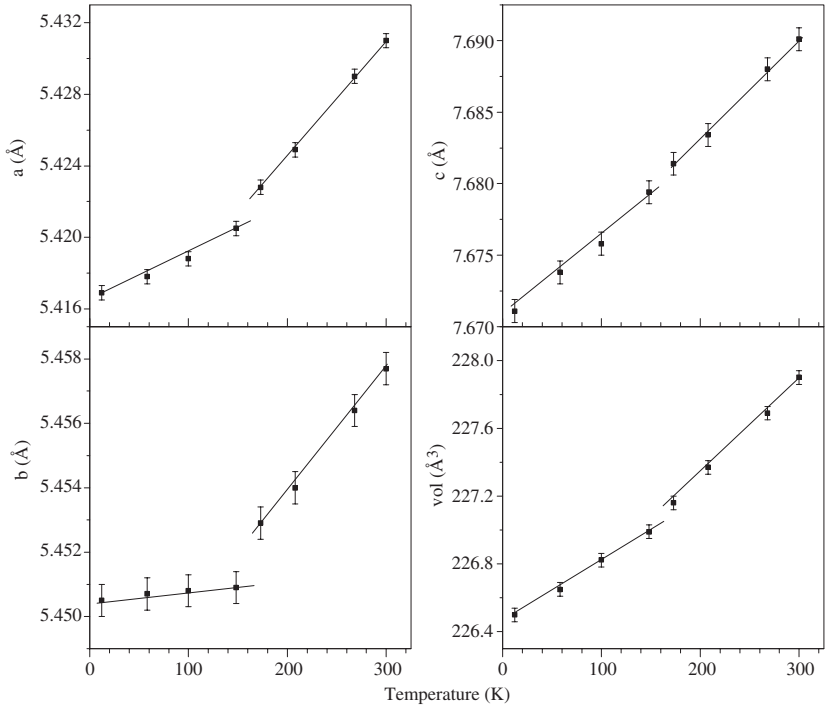

Figure 11. Variation of unit cell parameters as a function of temperature obtained after Rietveld refinement of powder XRD data for $Ca_{0.80}Pb_{0.20}TiO_3$.

CPT10, CPT20, CPT30 and CPT40 clearly indicates that the small peak in the $\varepsilon'(T)$ is not due to a ferroelectric or relaxor ferroelectric transition. In order to explore further the nature of the phase transition responsible for the peak in $\varepsilon'(T)$, we depict in figure 12 the variation of the dielectric stiffness $(1/\varepsilon')$ with temperature for the four CPT compositions. The linear dependence of $1/\varepsilon'$ on temperature above T'_m for all four compositions confirms that $\varepsilon'(T)$ follows a Curie–Weiss law, i.e.,

$$\varepsilon'(T) = C/[T - T_c] \tag{4}$$

where C is the Curie constant and T_c the Curie–Weiss temperature. The extrapolation of the straight line fit to the $1/\varepsilon'$ versus temperature data above T'_m to $1/\varepsilon' = 0$ gives T_c values of -110 , -87, -64 and -27 K for CPT10, CPT20, CPT30 and CPT40, respectively. Since the $\varepsilon'(T)$ data were available up to 300 K only on the higher temperature side, the temperature range over which the Curie–Weiss fit is depicted in figure 12 is somewhat smaller for CPT40. However, the linear fit is quite unambiguous as also is the negative value of the Curie–Weiss temperature T_c for all the compositions. The variation of T_c with composition is shown in figure 13. The values of T_c, as obtained by fitting Barrett's law (equation (1)) to the $\varepsilon'(T)$ data for all the compositions of figure 1, are also included in this figure for comparison. It is evident from this figure that the Curie–Weiss temperature becomes less and less negative with increasing x and would become positive for $x > 0.46$.

We shall now examine the possible origin of negative T_c in terms of Landau-type phenomenological theories which have been very successful in explaining second-order and weakly first-order ferroelectric [34] and antiferroelectric [35] phase transitions. For describing both the antiferroelectric and ferroelectric transitions, the free energy functional can be

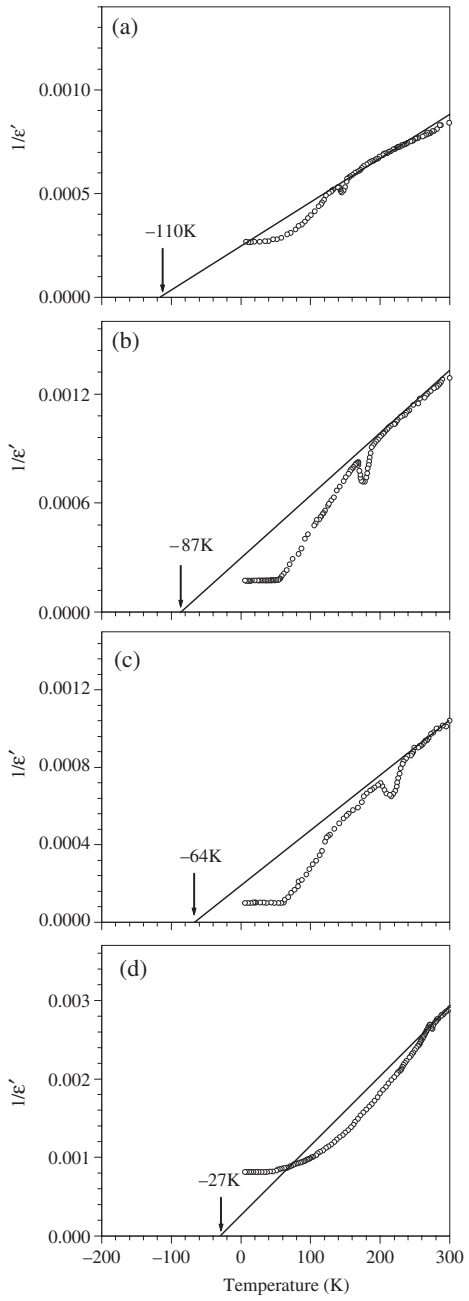

Figure 12. Curie–Weiss fits for $(Ca_{1-x}Pb_x)TiO_3$ with $x = 0.10, 0.20, 0.30$ and 0.40.

expanded in powers of the order parameter (i.e., polarization) as [36]

$$G(T, P_i, P_j) = G_0(T) + f(P_i^2 + P_j^2) + g P_i P_j + h(P_i^4 + P_j^4) + j(P_i^6 + P_j^6) \tag{5}$$

where P_i and P_j are the sublattice polarizations, $G_0(T)$ is the free energy density of the system in the paraelectric state ($P_i = P_j = 0$). The coefficients f, g, h and j are independent of P_i and P_j. g represents coupling between the sublattice polarizations P_i and P_j.

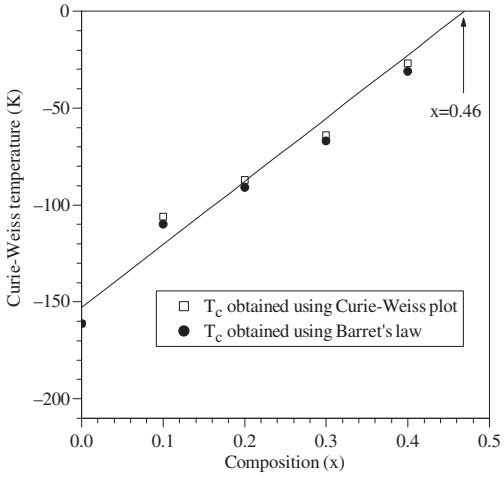

Figure 13. Variation of the Curie–Weiss temperature of $(Ca_{1-x}Pb_x)TiO_3$ with x, as obtained by Curie–Weiss (open squares) and Barrett fits (filled circles).

Taking $g = 0$, $P_i = P_j$, $f = a(T - T_c)$, where a is the inverse of the Curie–Weiss constant (C) and T_c is the Curie–Weiss temperature, the above free energy functional describes a ferroelectric transition for which the dielectric susceptibility follows the Curie–Weiss law (see equation (2)) for $T > T'_m$. For ferroelectric transitions T_c is necessarily positive [36].

The free energy functional given by equation (2) leads to an antiferroelectric phase transition for $P_i = -P_j$, $g \neq 0$ and with the following choice of temperature dependence for f [36]:

$$f = 1/2 + \lambda(T - T_o), \qquad \lambda = \text{constant}. \tag{6}$$

The susceptibility in the paraelectric phase ($T > T'_m$) now follows the following relationship [36]:

$$\chi' = [g + \lambda(T - T_o)]^{-1} \tag{7}$$

By choosing $C = 1/\lambda$ and $T_c = T_o - g/\lambda$, the above equation can be cast into the usual Curie–Weiss form for the dielectric permittivity given by equation (4) [22]. Thus for antiferroelectric phase transitions, the Curie–Weiss temperature $T_c = (T_o - g/\lambda)$ can be positive or negative depending upon the relative magnitudes of T_o and g/λ. For $g/\lambda > T_o$, T_c is obviously negative [22]. While a positive value of T_c can be linked with both ferroelectric and antiferroelectric transitions, a negative value of T_c is possible for antiferroelectric transitions only. The fact that the value of T_c gradually becomes less negative with increasing Pb^{2+} content in CPT (see figure 13) suggests that the strength of the sublattice coupling (g) is getting weaker with increasing Pb^{2+} content. When g eventually becomes zero on increasing the Pb^{2+} content further, it leads to a ferroelectric transition. This picture of an antiferroelectric transition with a negative T_c is consistent with the polarization studies also, which reveal the absence of a ferroelectric hysteresis loop for $0.10 \leqslant x \leqslant 0.40$, and its appearance for $x > 0.40$. Thus the negative value of the Curie–Weiss temperature and the absence of P–E hysteresis loop for $(Ca_{1-x}Pb_x)TiO_3$ with $0.10 \leqslant x \leqslant 0.40$ implies that the dielectric anomaly in figure 1 cannot be due to a ferroelectric transition but may be due to an antiferroelectric phase transition. This is similar to the case for the $(Ca_{1-x}Sr_x)TiO_3$ system where for compositions $0.88 < x \leqslant 0.40$, a negative value of T_c has been shown to be associated with an antiferroelectric

transition [19, 21, 22]. In magnetic systems also, a negative value of T_c is linked with an antiferromagnetic transition [37].

Important supporting evidence for the confirmation of an antiferroelectric phase transition missing in the present work is the observation of a double hysteresis loop [38]. For antiferroelectric materials, it is well known that the polarization induced by an external electric field is initially zero but the alternating dipoles switch at high fields leading to a field induced antiferroelectric to ferroelectric transition [38]. This leads to the appearance of the so-called double hysteresis loop. However, the absence of such a double P–E hysteresis loop is not surprising for ceramic samples of CPT. Even in the case of the well known antiferroelectric $PbZrO_3$, the double P–E loop could not be observed for ceramic samples at room temperature [39]. Double hysteresis loops characteristic of the antiferroelectric phase could be observed at room temperature only for single crystals [40] and oriented thin films [41] of $PbZrO_3$. It was later found that very high switching fields ($\sim$200 kV cm^{-1}) [41], which ceramic specimens cannot withstand because of their much lower breakdown strength due to the presence of pores, are required for observing the double hysteresis loop. We believe that the situation for CPT ceramic samples may be similar, and the observation of a double hysteresis loop has to await the availability of good quality single crystals or epitaxial thin films of this material.

3.4.2. Possible role of soft modes of $CaTiO_3$. The occurrence of an AFE phase transition usually leads to a doubling of the unit cell causing the appearance of new superlattice reflections as reported by Ranjan *et al* for $(Sr_{0.70}Ca_{0.30})TiO_3$ [19, 21]. But as said earlier, we did not observe any new superlattice peak in CPT below the transition temperatures for $0.10 \leqslant x \leqslant 0.40$. The non-observation of new superlattice peaks, however, does not necessarily preclude the possibility of an antiferroelectric phase transition in CPT, as explained in the following.

Zelezny *et al* [42] have reported softening without complete freezing of a low frequency zone boundary X E_g mode of the cubic phase of $CaTiO_3$. This mode originates from the X point $\left(q = \frac{1}{2}\ 0\ 0\right)$ of the zone boundary of the cubic phase, and involves primarily the O–Ti–O bending mode with Ti in alternating planes moving out of phase. Such a mode cannot lead to incipient ferroelectricity for which a soft zone centre optical mode is required. We believe that the Pb^{2+} substitution leads to freezing of this X E_g zone boundary soft mode causing antiparallel displacements of the Ti ions in alternating planes leading to an antiferroelectric phase with a negative Curie–Weiss temperature. The freezing of such a mode $\left(q = \frac{1}{2}\ 0\ 0\right)$ will not lead to any further cell doubling as the room temperature orthorhombic structure of CPT10 to CPT40 is already a doubled perovskite unit cell due to the freezing of the R $\left(q = \frac{1}{2}\ \frac{1}{2}\ \frac{1}{2}\right)$ and M $\left(q = \frac{1}{2}\ \frac{1}{2}\ 0\right)$ phonons occurring well above room temperature in the paraelectric state. Since there is no further cell doubling due to the freezing of the X E_g mode, new superlattice reflections are not expected. Thus even in the absence of new superlattice peaks in the low temperature XRD patterns of CPT ($0.10 \leqslant x \leqslant 0.40$), the anomalies in the dielectric permittivity shown in figure 1 and in the unit cell parameters shown in figure 11 could still be associated with an antiferroelectric phase transition if it is driven by the X E_g-like mode of the cubic phase.

The fact that the X E_g mode of pure $CaTiO_3$ does not completely freeze indicates some sort of incipient antiferroelectric instability. Zelezny *et al* [42] have shown that there is another low frequency soft mode whose eigenvectors are cubic zone centre $1\Gamma F_{1u}$ like. This suggests that $CaTiO_3$ has an incipient ferroelectric instability also, similar to those of $SrTiO_3$ [3] and $KTaO_3$ [1, 2]. The high dielectric permittivity of $CaTiO_3$ in the quantum saturation region (<50 K) points towards the involvement of such a zone centre optical phonon. The persistence

of the quantum saturation of the dielectric permittivity below 50 K even in the Pb^{2+} substituted samples suggests that the Pb^{2+} substitution facilitates the freezing of the zone boundary X E_g mode but not the zone centre soft mode.

4. Concluding remarks

We have shown that Pb^{2+} substitution leads to a dielectric anomaly in $(Ca_{1-x}Pb_x)TiO_3$ ceramics for the composition range $0.10 \leqslant x \leqslant 0.40$. This dielectric anomaly is superposed on a continuously rising $\varepsilon'(T)$ background which shows quantum saturation below 50 K similar to that of pure $CaTiO_3$. Fitting the Curie–Weiss law and Barrett's law to the $\varepsilon'(T)$ data gives a negative Curie–Weiss temperature. The negative Curie–Weiss temperature rules out any ferroelectric transition but can be rationalized in terms of an antiferroelectric phase transition using Kittel's phenomenological theory of antiferroelectric transitions. Additional evidence for the new phase transition comes from the observation of anomalies in the unit cell parameters obtained by temperature dependent x-ray diffraction experiments and the excess '$1/f$' conductance noise measurements at the transition temperature. The nature of the phase transition changes abruptly around $x = 0.45$ and a relaxor ferroelectric-type behaviour is observed for $0.45 \leqslant x < 0.60$. For $x > 0.60$, a normal ferroelectric transition is observed. Results presented in this paper show that for $0.10 \leqslant x \leqslant 0.40$ and $x \geqslant 0.65$, the antiferroelectric and ferroelectric instabilities, respectively, dominate whereas for the intermediate compositions, $0.40 \leqslant x < 0.65$, the two instabilities compete giving rise to a relaxor ferroelectric-type behaviour due to frustration [19]. The ferroelectric and the antiferroelectric instabilities in this mixed system seem to stem from the $PbTiO_3$ and $CaTiO_3$ ends, respectively.

Acknowledgments

We thank Professor T V Ramakrishnan, FRS, for his interest, fruitful discussions and a critical reading of the first version of the paper. Amreesh Chandra is grateful to CSIR, India, for the award of a Senior Research Fellowship. DP acknowledges partial support from IUC-DAEF, Mumbai Centre, for this work. Rajeev Ranjan acknowledges the Department of Science and Technology, Government of India, for financial support.

References

[1] Vugmeister B E and Glinchuk M D 1990 *Rev. Mod. Phys.* **62** 993
[2] Hochli U T, Knorr K and Loidl A 1990 *Adv. Phys.* **39** 405
[3] Muller K A and Burkard H 1979 *Phys. Rev.* B **19** 3593
[4] Kim I S, Itoh M and Nakamura T J 1992 *Solid State Chem.* **101** 77
[5] Samara G A and Peercy P S 1973 *Phys. Rev.* B **7** 1131
[6] Shan Y J, Nakamura T, Inaguma Y and Itoh M 1998 *Solid State Ion.* **108** 123
[7] Buchanan R C 1986 *Ceramic Materials for Electronics* (New York: Dekker)
[8] Muller K A, Berlinger W and Tosati E 1991 *Z. Phys.* B **84** 277
[9] Vacher R, Pelous J, Hennion B, Coddens G, Courtens E and Muller K A 1992 *Europhys. Lett.* **17** 45
[10] Nes O M, Muller K A, Suzuki T and Fossheim F 1992 *Europhys. Lett.* **19** 397
[11] Viana R, Lukenheimer P, Hemberger J, Bohmer R and Loidl A 1994 *Phys. Rev.* B **50** 601
[12] Martonak R and Tossatti E 1994 *Phys. Rev.* B **49** 12596
[13] Schneider T, Beck H and Stoll E 1976 *Phys. Rev.* B **13** 1123
[14] Zhong W and Vanderbilt D 1996 *Phys. Rev.* B **53** 5047
Roussev R and Mills A J 2003 *Phys. Rev.* B **67** 014105
[15] Barrett J H 1952 *Phys. Rev.* **86** 118

[16] Rytz D, Höchli U T and Bilz H 1980 *Phys. Rev.* B **22** 359
[17] Bednorz J G and Muller K A 1984 *Phys. Rev. Lett.* **52** 2289
[18] Lemanov V V, Smirnova E P, Syrnikov P P and Tarakanov E A 1996 *Phys. Rev.* B **54** 3151
Lemanov V V, Smirnova E P, Syrnikov P P and Tarakanov E A 1997 *Phys. Solid State* **39** 628
[19] Ranjan R, Pandey D and Lalla N P 2000 *Phys. Rev. Lett.* **84** 726
[20] Ouillon R, Lucarre J P P, Ranson P, Pruzan P, Mishra S K, Ranjan R and Pandey D 2002 *J. Phys.: Condens. Matter* **14** 2079
[21] Ranjan R and Pandey D 2001 *J. Phys.: Condens. Matter* **13** 4239
[22] Ranjan R and Pandey D 2001 *J. Phys.: Condens. Matter* **13** 4251
[23] Shirane G and Yamada Y 1969 *Phys. Rev.* **177** 858
[24] Perry C H and McNelly T F 1967 *Phys. Rev.* **154** 465
[25] Lemanov V V, Sotnikov A V, Smirnova E P, Weihnacht M and Kunze R 1999 *Solid State Commun.* **110** 611
[26] Lemanov V V, Sotnikov A V, Smirnova E P and Weihnacht M 2002 *Appl. Phys. Lett.* **81** 886
[27] Ranjan R, Singh N, Pandey D, Siruguri V, Krishna P S R, Paranjpe S K and Banerjee A 1997 *Appl. Phys. Lett.* **70** 3221
[28] Jaffe B, Cook W Jr and Jaffe H 1971 *Piezoelectric Ceramics* (New York: Academic)
[29] Pandey D 1995 *Key Eng. Mater.* **101/102** 177
[30] Cross L E 1987 *Ferroelectrics* **76** 241
[31] Tagantsev A K 1994 *Phys. Rev. Lett.* **72** 1100
[32] Glazer A M 1972 *Acta Crystallogr.* B **28** 3384
Glazer A M 1975 *Acta Crystallogr.* A **31** 756
[33] Chandra A and Pandey D 2003 *J. Mater. Res.* **18** 413
[34] Devonshire A F 1949 *Phil. Mag.* **40** 1040
Devonshire A F 1951 *Phil. Mag.* **42** 1065
[35] Pokharel B P and Pandey D 2002 *Phys. Rev.* B **65** 214108
[36] Blinc R and Zeks B 1974 *Soft Modes in Ferroelectrics and Antiferroelectrics* (Amsterdam: North-Holland)
[37] Kittel C 1996 *Introduction to Solid State Physics* (Singapore: Wiley)
[38] Lines M E and Glass A M 1977 *Principles and Applications of Ferroelectrics and Related Materials* (Oxford: Clarendon)
[39] Shirane G, Sawaguchi E and Takagi Y 1951 *Phys. Rev.* **84** 476
[40] Fesenko O E, Kolesova R V and Sindeyev Y G 1978 *Ferroelectrics* **20** 177
[41] Tani T, Li J F, Viehland D and Payne D A 1994 *J. Appl. Phys.* **75** 3017
[42] Zelezny V, Cockayne E, Petzelt J, Limonov M F, Usvyat D E, Lemanov V V and Volkov A A 2002 *Phys. Rev.* B **66** 224303